

Chapter 7

A photometric search for clouds on Titan

7.1 Introduction

Variations in Titan's flux as a function of orbital phase provided the first reliable evidence of a heterogeneous surface in synchronous rotation with Titan's 15.9 day orbit. Titan's rotational lightcurve is only expressed at wavelengths of low methane opacity (spectral windows to the surface), while the flux in the methane bands, due only to sunlight scattered by the stratospheric haze, remains unchanging on this timescale. By dividing the measured flux in a window region by that in a nearby methane band, lightcurves at 1.1, 1.3, 1.6, and 2.0 μm have been derived (Lemmon *et al.*, 1993; Griffith, 1993; Coustenis *et al.*, 1995). Correcting for systematic offsets in the geometric albedo reported by various observers, Lemmon *et al.* (1995) found that Titan's lightcurve repeats from one rotation to the next, to the 5% precision of the data then available. More precise spectral observations have since uncovered transient methane clouds in Titan's troposphere, which superimpose daily $\sim 3\%$ (at 2 μm), and occasionally larger, variations on the rotational lightcurve (Griffith *et al.*, 1998, 2000).

High resolution imaging studies of Titan in the visible (Smith *et al.*, 1996; Richardson *et al.*, 2001; Bouchez *et al.*, 2003) and near-infrared (Combes *et al.*, 1997; Gibbard *et al.*, 1999; Meier *et al.*, 2000; Coustenis *et al.*, 2001) revealed the surface albedo features which give rise to Titan's repeating lightcurve, but long failed to conclusively detect clouds. Recent adaptive optics observations with the Keck and Gemini telescopes, performed soon after the observations described in this chapter were begun, have located Titan's daily clouds

near the south pole (Brown *et al.*, 2002; Roe *et al.*, 2002). Individual storms were observed to persist at least 24 hours in one case (Brown *et al.*, 2002), and vary in flux by 50% over 3 hr in another (Roe *et al.*, 2002), but little other information on their lifetimes, formation frequency, and size spectrum can be gleaned from these few observations (a total of 10 nights.)

Frequent observations over many rotations, either resolved imaging or photometric monitoring, provide the only means of constraining many of these basic properties of Titan's transient clouds. We began nightly photometry of Titan on 5 December 2001, using a 14-inch telescope on the Caltech campus to measure the relative albedo of Titan's lower atmosphere and surface at 750 and 825 nm. Ideally, such a study would be performed in the near-infrared (e.g., the 1.6 or 2.0 μm spectral windows), where the low optical depth of stratospheric haze maximizes the amplitude of Titan's rotational lightcurve (Lemmon *et al.*, 1995), and the photometric effect of any transient clouds. However, available equipment limited us to wavelengths shorter than 1 μm , while variable atmospheric water absorptions ruled out the 950 nm transmission window. The optical depth of Titan's stratospheric haze may be as high as $\tau = 6$ at 750 nm (Rannou *et al.*, 1995), but the high single-scattering albedo of the aerosols (McKay *et al.*, 2001) allows Titan's surface to be detected nevertheless, albeit with low contrast (Smith *et al.*, 1996; Richardson *et al.*, 2001).

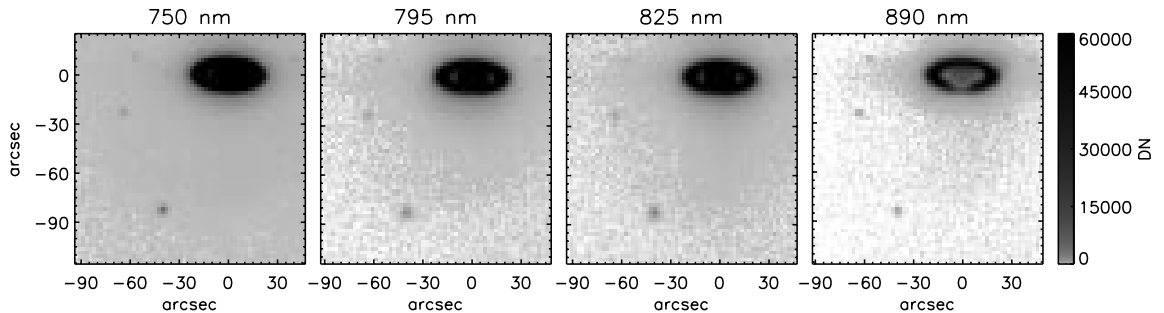


Figure 7.1: A series of 4 consecutive images of Titan taken on 02 February 2002, between 03:57:55 and 03:58:27 UT. Titan is the brightest of the 4 visible satellites, $90''$ south-east of Saturn. Raw 5 s integrations have been corrected for detector bias and pixel gain variations. A logarithmic gray-scale highlights the scattered light from Saturn, brightest in the shorter wavelength filters.

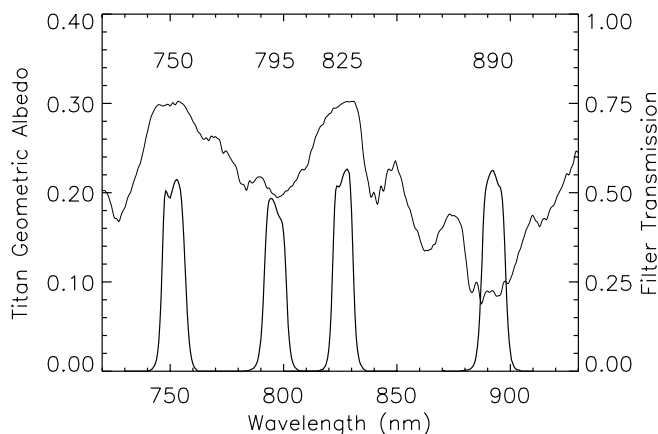


Figure 7.2: Transmission spectra of filters used on the 14-inch telescopes, superimposed on a spectrum of Titan from Karkoschka (1998). Titan is bright where CH_4 opacity is low, and dark in the CH_4 bands at 795 and 890 nm.

7.2 Observations

Photometric observations of Titan were acquired on 81 nights between 5 December 2001 to 12 April 2002, using the 14-inch Celestron Schmidt-Cassegrain telescope of the Robinson-Downs Rooftop Observatory. We recorded the images of Titan on a 512^2 pixel Kodak CCD detector (Santa Barbara Instruments Group camera model ST-9E), with a native platescale of $1.1'' \text{ pix}^{-1}$. Between 80 and 400 images were acquired each night, with integration times of 5 s or 10 s, depending on seeing conditions and cloud opacity. Seeing was generally 4–5'' FWHM, and the weather conditions ranged from clear (46% of the nights) to partly cloudy. To maximize the observing efficiency, images were rebinned by a factor of 2, and only the smallest possible subarray containing both Saturn and Titan was read out, generally 96×64 binned pixels. A summary of the observations is provided in Table 7.1.

Four narrow-band filters between 750 nm and 890 nm were used to sample Titan's spectrum, two centered on CH_4 absorption bands and two centered on window regions of low CH_4 opacity (Fig. 7.2). Titan's atmosphere is opaque below ~ 80 km altitude in both the 795 nm and 890 nm filters, and thus the only light detected is scattered off the stratospheric haze, which we expect to vary only on seasonal timescales. We therefore used Titan's flux in the CH_4 bands as our photometric standards, alternating images taken at window wavelengths (750 nm and 825 nm) with those taken in the CH_4 bands (795 nm and 890 nm), and dividing the consecutively measured fluxes. We typically cycled through

Table 7.1: C-14 observations. I.

Date	UT	Exp.	Lon.	Lat.	Airmass	750/795	N	825/890	N	795/890	N
05 Dec 2001	06:05–06:43	10.0	112.4	-25.6	1.10–1.05	2.496 ± 0.008	25	1.234 ± 0.004	25	4.131 ± 0.037	25
06 Dec 2001	05:48–06:18	10.0	134.7	-25.6	1.12–1.07	2.434 ± 0.033	20	1.139 ± 0.025	20	3.673 ± 0.134	20
07 Dec 2001	05:48–06:27	10.0	157.5	-25.6	1.11–1.06	2.471 ± 0.012	25	1.196 ± 0.004	25	4.031 ± 0.060	25
13 Dec 2001	04:32–04:59	10.0	292.3	-25.5	1.23–1.16	2.471 ± 0.008	20	1.200 ± 0.005	20	4.076 ± 0.036	20
14 Dec 2001	06:08–06:35	10.0	316.5	-25.5	1.05–1.03	2.105 ± 0.060	12	1.111 ± 0.030	12	3.147 ± 0.268	7
16 Dec 2001	04:48–05:14	10.0	0.4	-25.5	1.16–1.11	2.478 ± 0.017	20	1.167 ± 0.007	20	3.888 ± 0.060	20
17 Dec 2001	05:49–06:21	10.0	24.1	-25.5	1.05–1.03	2.491 ± 0.017	25	1.234 ± 0.018	25	4.158 ± 0.057	25
18 Dec 2001	05:22–05:50	10.0	46.3	-25.5	1.08–1.05	2.519 ± 0.007	20	1.257 ± 0.005	20	4.244 ± 0.035	20
19 Dec 2001	06:41–07:15	10.0	70.2	-25.5	1.03–1.04	2.505 ± 0.007	25	1.269 ± 0.004	25	4.342 ± 0.035	25
20 Dec 2001	05:48–06:16	10.0	92.0	-25.5	1.05–1.03	1.171 ± 1.448	9	0.577 ± 0.528	13	2.333 ± 2.438	12
23 Dec 2001	07:40–08:04	10.0	161.8	-25.5	1.08–1.12	2.465 ± 0.014	18	1.163 ± 0.008	18	3.972 ± 0.077	18
25 Dec 2001	05:15–05:42	10.0	204.9	-25.5	1.05–1.04	2.437 ± 0.009	20	1.186 ± 0.012	20	4.010 ± 0.048	20
04 Jan 2002	05:02–05:29	10.0	71.0	-25.5	1.04–1.03	2.476 ± 0.017	20	1.237 ± 0.007	20	4.168 ± 0.064	20
05 Jan 2002	05:05–05:34	10.0	93.8	-25.5	1.03–1.03	2.504 ± 0.016	21	1.223 ± 0.007	21	4.256 ± 0.058	21
06 Jan 2002	05:08–05:35	10.0	116.4	-25.5	1.03–1.03	2.550 ± 0.015	20	1.244 ± 0.008	20	4.241 ± 0.063	20
11 Jan 2002	04:60–05:27	10.0	229.6	-25.5	1.03–1.04	2.456 ± 0.011	20	1.209 ± 0.007	20	4.126 ± 0.047	20
13 Jan 2002	05:01–05:36	10.0	274.9	-25.5	1.03–1.05	2.433 ± 0.027	25	1.186 ± 0.018	25	3.980 ± 0.057	25
14 Jan 2002	04:43–05:10	10.0	297.2	-25.5	1.03–1.03	2.503 ± 0.011	20	1.244 ± 0.005	20	4.148 ± 0.061	20
17 Jan 2002	04:35–05:02	10.0	4.9	-25.4	1.03–1.04	2.467 ± 0.014	20	1.199 ± 0.008	20	4.206 ± 0.123	20
18 Jan 2002	02:51–05:08	10.0	26.8	-25.5	1.11–1.04	2.494 ± 0.005	100	1.229 ± 0.003	100	4.231 ± 0.025	60
19 Jan 2002	07:10–07:42	10.0	52.5	-25.5	1.28–1.42	2.519 ± 0.011	40	1.277 ± 0.005	40	0.000 ± 0.000	0
20 Jan 2002	04:48–05:13	10.0	72.9	-25.5	1.04–1.05	2.516 ± 0.007	30	1.252 ± 0.004	30	0.000 ± 0.000	0
21 Jan 2002	04:40–05:06	10.0	95.4	-25.5	1.03–1.05	2.536 ± 0.004	30	1.255 ± 0.003	30	0.000 ± 0.000	0
22 Jan 2002	04:01–05:05	10.0	117.7	-25.5	1.03–1.05	2.543 ± 0.005	60	1.254 ± 0.002	60	4.320 ± 0.022	60
23 Jan 2002	03:40–06:11	5.0	141.2	-25.5	1.04–1.16	1.996 ± 0.226	30	1.026 ± 0.136	25	2.681 ± 0.809	5
24 Jan 2002	04:45–05:29	10.0	163.5	-25.5	1.04–1.09	2.425 ± 0.010	40	1.246 ± 0.005	40	4.176 ± 0.041	40
25 Jan 2002	04:35–05:31	10.0	186.0	-25.5	1.04–1.09	2.506 ± 0.010	50	1.258 ± 0.005	50	4.116 ± 0.030	50
26 Jan 2002	02:20–03:21	5.0	206.6	-25.5	1.11–1.04	2.475 ± 0.010	45	1.230 ± 0.006	45	4.090 ± 0.064	45
30 Jan 2002	04:29–05:13	10.0	298.9	-25.5	1.05–1.10	2.553 ± 0.010	40	1.259 ± 0.006	40	4.181 ± 0.049	40
31 Jan 2002	03:37–04:25	10.0	320.6	-25.5	1.03–1.05	2.481 ± 0.007	40	1.240 ± 0.004	40	4.088 ± 0.036	40

Table 7.1: C-14 observations. II.

Date	UT	Exp.	Lon.	Lat.	Airmass	750/795	N	825/890	N	795/890	N
01 Feb 2002	04:22–05:06	10.0	343.9	-25.5	1.05–1.10	2.464 ± 0.009	39	1.216 ± 0.003	39	4.159 ± 0.030	39
02 Feb 2002	03:57–04:40	5.0	6.1	-25.5	1.04–1.07	2.484 ± 0.007	60	1.244 ± 0.004	60	4.316 ± 0.035	60
03 Feb 2002	02:53–03:47	10.0	27.7	-25.5	1.04–1.03	2.515 ± 0.006	50	1.268 ± 0.003	50	4.320 ± 0.027	50
04 Feb 2002	05:00–05:53	10.0	52.3	-25.5	1.11–1.24	2.553 ± 0.006	50	1.273 ± 0.004	50	4.370 ± 0.027	50
06 Feb 2002	02:21–03:23	10.0	95.0	-25.5	1.05–1.03	2.505 ± 0.005	55	1.277 ± 0.003	55	4.300 ± 0.025	55
07 Feb 2002	02:05–02:58	10.0	117.3	-25.5	1.06–1.03	2.504 ± 0.005	50	1.275 ± 0.003	50	4.236 ± 0.026	50
08 Feb 2002	02:24–03:06	10.0	140.1	-25.5	1.04–1.03	2.484 ± 0.008	40	1.228 ± 0.004	40	4.237 ± 0.035	40
09 Feb 2002	02:38–03:20	10.0	162.9	-25.5	1.04–1.03	2.454 ± 0.009	40	1.169 ± 0.005	40	3.944 ± 0.045	40
10 Feb 2002	02:38–03:22	10.0	185.5	-25.5	1.03–1.03	2.520 ± 0.009	41	1.268 ± 0.005	41	4.075 ± 0.043	41
11 Feb 2002	02:08–03:12	10.0	207.8	-25.5	1.05–1.03	2.464 ± 0.006	60	1.235 ± 0.003	60	4.129 ± 0.025	60
12 Feb 2002	02:26–03:47	5.0	230.8	-25.5	1.04–1.06	2.427 ± 0.030	58	1.200 ± 0.013	58	3.815 ± 0.109	58
13 Feb 2002	02:35–03:17	10.0	253.2	-25.5	1.03–1.04	2.261 ± 0.036	40	1.188 ± 0.017	40	3.059 ± 0.144	40
15 Feb 2002	03:11–03:48	5.0	298.8	-25.5	1.04–1.07	2.528 ± 0.032	50	1.168 ± 0.014	50	3.725 ± 0.102	50
16 Feb 2002	03:12–03:48	5.0	321.4	-25.5	1.04–1.07	2.492 ± 0.012	50	1.191 ± 0.008	50	4.037 ± 0.049	50
18 Feb 2002	02:04–02:43	5.0	5.3	-25.5	1.03–1.03	1.570 ± 0.308	40	1.203 ± 0.063	36	3.119 ± 0.463	30
19 Feb 2002	02:50–03:27	5.0	28.6	-25.5	1.04–1.06	2.500 ± 0.010	49	1.225 ± 0.008	50	4.124 ± 0.065	50
20 Feb 2002	02:47–03:21	5.0	51.1	-25.6	1.04–1.06	2.539 ± 0.036	50	1.189 ± 0.020	50	3.904 ± 0.119	42
22 Feb 2002	02:26–03:19	10.0	96.0	-25.6	1.03–1.07	2.559 ± 0.006	50	1.225 ± 0.003	50	4.305 ± 0.028	50
23 Feb 2002	02:11–03:48	10.0	118.7	-25.6	1.03–1.11	2.554 ± 0.008	90	1.277 ± 0.004	90	4.281 ± 0.032	90
24 Feb 2002	02:08–03:11	10.0	140.9	-25.6	1.03–1.07	2.497 ± 0.007	60	1.207 ± 0.004	60	4.091 ± 0.031	60
25 Feb 2002	02:32–03:19	10.0	163.7	-25.6	1.04–1.08	2.532 ± 0.013	40	1.236 ± 0.005	40	4.001 ± 0.037	40
26 Feb 2002	02:08–03:20	5.0	186.1	-25.6	1.03–1.09	2.483 ± 0.009	100	1.204 ± 0.005	100	3.971 ± 0.032	100
28 Feb 2002	02:12–03:05	10.0	231.1	-25.6	1.03–1.08	2.526 ± 0.007	50	1.210 ± 0.004	50	4.086 ± 0.035	50
02 Mar 2002	02:12–03:33	10.0	276.4	-25.6	1.04–1.14	2.512 ± 0.008	75	1.199 ± 0.004	75	4.052 ± 0.031	75
03 Mar 2002	02:38–03:48	10.0	299.3	-25.6	1.06–1.18	2.513 ± 0.006	60	1.248 ± 0.004	60	4.155 ± 0.032	60
04 Mar 2002	02:16–03:09	10.0	321.3	-25.6	1.04–1.10	2.515 ± 0.007	50	1.263 ± 0.004	50	4.192 ± 0.031	50
05 Mar 2002	02:17–03:17	10.0	343.9	-25.7	1.05–1.13	2.505 ± 0.006	57	1.233 ± 0.003	57	4.178 ± 0.023	57
06 Mar 2002	02:44–03:56	5.0	6.9	-25.7	1.08–1.23	2.494 ± 0.011	100	1.189 ± 0.005	100	4.038 ± 0.047	100
11 Mar 2002	02:41–03:48	10.0	119.4	-25.7	1.10–1.27	2.600 ± 0.010	63	1.236 ± 0.005	63	4.324 ± 0.035	63
12 Mar 2002	02:21–03:51	10.0	141.7	-25.8	1.08–1.29	2.529 ± 0.009	83	1.192 ± 0.004	83	4.106 ± 0.035	83

Table 7.1: C-14 observations. III.

Date	UT	Exp.	Lon.	Lat.	Airmass	750/795	N	825/890	N	795/890	N
13 Mar 2002	02:23–03:35	5.0	164.2	-25.8	1.08–1.25	2.501 ± 0.009	100	1.172 ± 0.005	100	4.075 ± 0.042	100
14 Mar 2002	02:26–03:35	10.0	186.7	-25.8	1.09–1.26	2.454 ± 0.010	65	1.247 ± 0.005	65	4.056 ± 0.035	65
15 Mar 2002	02:31–03:25	10.0	209.2	-25.8	1.11–1.24	2.520 ± 0.007	50	1.215 ± 0.004	50	4.140 ± 0.025	50
16 Mar 2002	02:27–03:20	10.0	231.7	-25.8	1.11–1.24	2.517 ± 0.007	50	1.202 ± 0.005	50	4.205 ± 0.039	50
17 Mar 2002	02:45–03:57	10.0	254.6	-25.8	1.15–1.39	2.480 ± 0.010	66	1.197 ± 0.006	66	3.862 ± 0.041	66
19 Mar 2002	03:29–04:21	10.0	300.1	-25.8	1.30–1.58	2.512 ± 0.012	50	1.229 ± 0.007	50	4.047 ± 0.035	50
20 Mar 2002	03:13–04:18	10.0	322.5	-25.8	1.26–1.58	2.523 ± 0.010	60	1.227 ± 0.005	60	4.054 ± 0.037	60
21 Mar 2002	02:46–04:27	5.0	344.8	-25.8	1.19–1.68	2.448 ± 0.025	140	1.171 ± 0.010	140	3.050 ± 0.320	140
22 Mar 2002	03:52–04:44	10.0	7.9	-25.8	1.46–1.87	2.519 ± 0.010	50	1.231 ± 0.006	50	3.917 ± 0.036	50
23 Mar 2002	03:21–03:50	10.0	29.7	-25.8	1.33–1.47	2.555 ± 0.015	27	1.204 ± 0.015	27	4.110 ± 0.063	26
25 Mar 2002	04:13–05:07	10.0	75.7	-25.9	1.68–2.33	2.532 ± 0.015	50	1.187 ± 0.007	50	3.965 ± 0.065	50
26 Mar 2002	03:45–04:25	5.0	97.6	-25.9	1.51–1.81	1.698 ± 0.209	36	0.800 ± 0.106	33	1.224 ± 2.296	10
27 Mar 2002	02:35–03:55	10.0	119.4	-25.9	1.22–1.60	2.597 ± 0.007	75	1.255 ± 0.004	75	4.314 ± 0.034	75
31 Mar 2002	03:27–04:09	10.0	209.9	-26.0	1.50–1.84	2.507 ± 0.015	40	1.189 ± 0.009	40	3.701 ± 0.085	40
01 Apr 2002	02:55–03:50	10.0	232.0	-26.0	1.36–1.69	2.486 ± 0.013	50	1.179 ± 0.008	50	4.005 ± 0.052	50
02 Apr 2002	03:08–03:51	10.0	254.6	-26.0	1.44–1.74	2.380 ± 0.017	40	1.186 ± 0.011	40	3.660 ± 0.082	40
05 Apr 2002	02:40–03:45	10.0	321.7	-26.0	1.35–1.78	2.516 ± 0.012	60	1.212 ± 0.006	60	3.938 ± 0.042	60
09 Apr 2002	02:49–03:31	10.0	51.5	-26.0	1.47–1.78	2.585 ± 0.015	40	1.206 ± 0.008	40	4.059 ± 0.076	40
10 Apr 2002	02:52–03:46	5.0	74.1	-26.0	1.50–1.98	2.519 ± 0.017	75	1.202 ± 0.011	75	3.884 ± 0.093	75
11 Apr 2002	02:53–03:41	10.0	96.5	-26.0	1.53–1.95	2.566 ± 0.018	45	1.198 ± 0.010	45	3.991 ± 0.065	45
12 Apr 2002	02:52–03:45	10.0	119.0	-26.1	1.55–2.05	2.570 ± 0.020	50	1.173 ± 0.009	50	3.775 ± 0.079	50

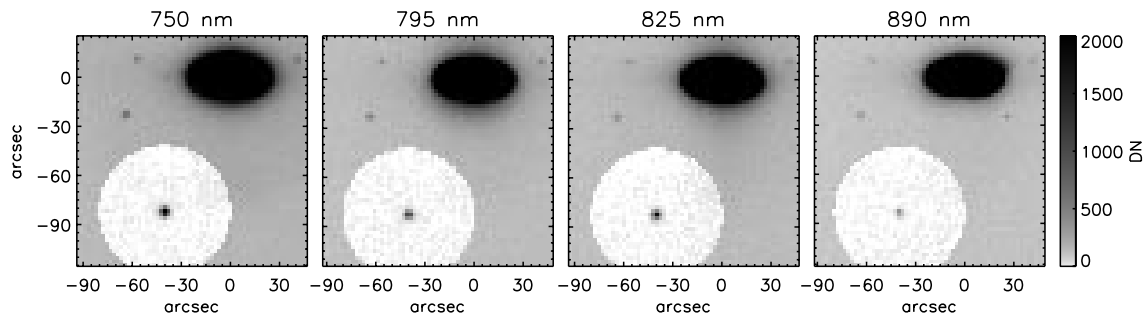


Figure 7.3: Same images as displayed in Fig. 7.1, but with Saturn’s scattered light subtracted from the region surrounding Titan.

the 4 filters in order of ascending wavelength, completing a cycle of 4 exposures every 65 s (every 42 s when using 5 s integrations.)

7.3 Data reduction

Each image was corrected for the detector bias and dark current by subtracting a median of identical exposure dark frames taken the same night. Pixel-to-pixel gain variations were then compensated for by dividing each image by the mean of a set of daytime sky images taken once per month. A strong halo of scattered light surrounds Saturn’s image on the detector and extends to Titan’s vicinity, at a level of $\sim 5\%$ Titan’s peak intensity (Fig. 7.1.) This effect is probably due to the highly reflective front surface of the interference filters used in these observations. To correct for the scattered light superimposed on Titan’s image, we make the assumption that its intensity is radially symmetric about Saturn’s position on the detector, and fit a 4th order polynomial to the background in an annulus $10''$ – $40''$ around Titan. We then subtract this model of the background light from the entire region within $40''$ of Titan’s location (Fig. 7.3.)

We computed Titan’s instrumental magnitude in each image by summing the counts within an aperture centered on Titan’s apparent position. The aperture radius was chosen by computing a nightly-mean PSF in each filter and determining the aperture necessary to sample 99.8% of its light, generally $8''$ – $12''$. The signal to noise ratio of the resulting photometric measurement ranged from 100 (750 nm) to 15 (890 nm) on clear nights. Figure 7.4 displays the measured instrumental flux of Titan in all four filters on typical clear and partly-cloudy nights.

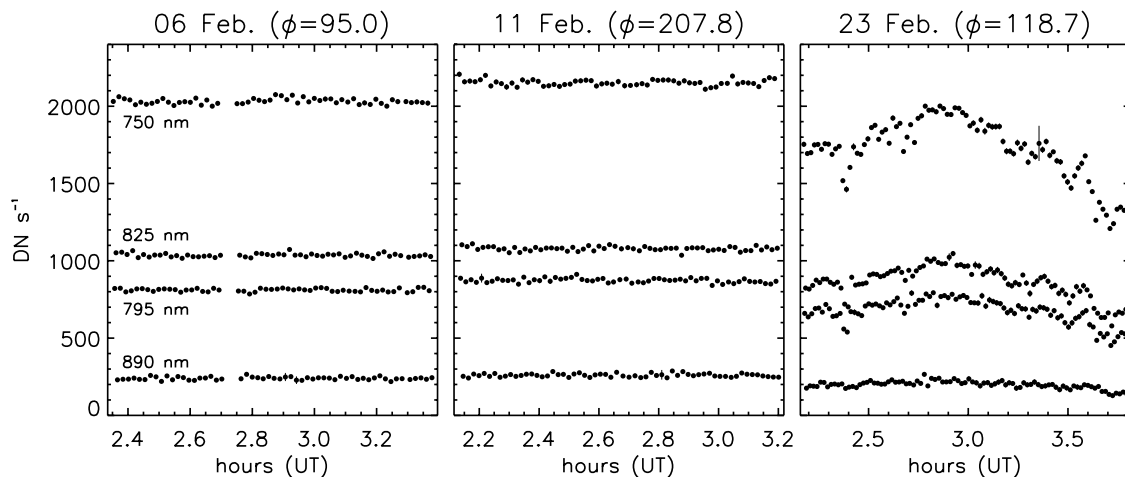


Figure 7.4: Photometry of Titan in four filters on three nights in February 2002. These nights were chosen to illustrate both clear and cloudy conditions, and to sample Titan’s leading (6 and 23 February) and trailing (11 February) faces. Though we detect the surface albedo contrasts in the flux ratios (Fig. 7.5), the absolute flux variations seen here are due to changing extinction and clouds. The 1- σ error bars displayed include only the random error due to electronic and photon noise.

The purpose of alternating rapidly between surface-sensitive and CH₄ band filters is to calibrate out opacity variations imposed by atmospheric extinction and clouds on Earth. In practice, we cannot sample the photometry at a sufficiently high rate to keep up with the opacity variations of passing clouds. However, averaged over a sufficiently long period and assuming the opacity is not increasing or decreasing monotonically, the errors average out and the correct flux ratio can be recovered. There remains the concern that the clouds or other sources of opacity might redden Titan’s spectrum, mimicking a change in surface albedo or cloud cover on Titan. This effect proves to be important in several filter ratios, and we correct for it below.

Having determined Titan’s instrumental flux at 4 wavelengths, 6 possible flux ratios can be computed. The flux ratios 750/795 nm, 825/795 nm, and 825/890 nm record the albedo of Titan’s surface and lower atmosphere, relative to that of the overlying haze. We disregard 750/890 nm as it is the most prone to the reddening previously mentioned. The flux ratio 750/825 nm compares the two surface-probing wavelengths, potentially allowing changes in the color of the lower atmosphere and surface to be detected. Similarly, the CH₄ band ratio 795/890 nm measures the color of the stratospheric haze. The most useful of these flux

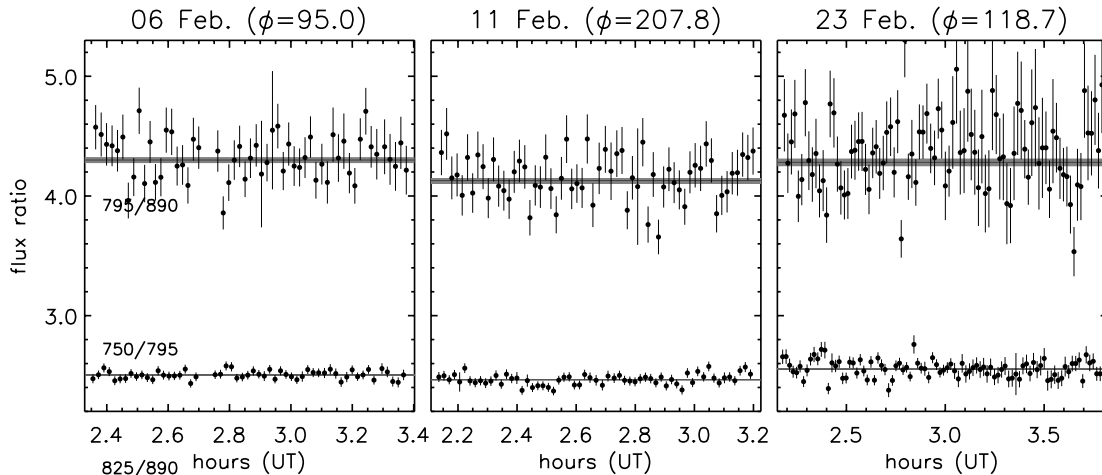


Figure 7.5: Ratio of Titan’s flux in alternating filters, on the same nights as displayed in Fig. 7.4. The nightly mean flux ratio, and its $1\text{-}\sigma$ uncertainty, are indicated by the horizontal lines and gray bands. Note that while the surface-sensitive flux ratios 750/795 nm and 825/890 nm vary with rotational phase ϕ , the CH_4 band ratio 795/890 nm remains unchanged.

ratios proved to be 750/795 nm and 825/890 nm, providing two independent measurements of changes in the albedo of Titan’s lower atmosphere and surface, and 795/890 nm as a control. We display time series of these three flux ratios in Fig. 7.5, for the same nights as the raw photometry in Fig. 7.4.

The final step of the initial data reduction process is to compute the weighted mean of each series of flux ratios for every night. The dominant source of uncertainty in the flux ratio estimate on cloudy nights is the temporal variation terrestrial cloud opacity between consecutive observations in the two filters. We therefore adopt the standard deviation of the measured flux ratios as our estimate of their uncertainty. On partly-cloudy nights, this is typically several times larger than the uncertainty expected from electronic and photon noise alone. We reject occasional outliers whose deviation from the weighted mean of that night is greater than 2σ (generally due to a cosmic ray hit within the photometric aperture). Taking a weighted average of the remaining flux ratios, we reduce the night’s observations to the mean values of the following 3 flux ratios with associated uncertainties: 750/795 nm, 825/890 nm, and 795/890 nm. Nights on which the signal to noise ratio of the 825/890 nm mean was less than 60.0 were then excluded from further study, leaving 60 nights.

Rapidly alternating between filters and ratioing Titan’s flux between them compensates

for correlated changes in flux between the filters, but it does not correct variable wavelength-dependent opacity. Though terrestrial clouds are generally assumed to be “gray” due to their large particle size, this may not be true at the level of a 1% flux ratio over 50 nm. Furthermore, several of our filters include H₂O absorption bands which may vary in opacity as a function of humidity. Though we did not observe any photometric standards, we can roughly estimate the mean extinction on each night by comparing Titan’s raw 795 nm flux (in DN s⁻¹) recorded each of the 81 nights. As Fig. 7.6 illustrates, the measured 795 nm flux is dominated by the Earth’s gradual recession from Titan, California’s cyclic weather patterns, and the increasing airmass of the observations during the final 4 weeks of the project. Scaling Titan’s predicted flux to match that observed on what was apparently the clearest night of the entire project (11 Feb 2002), we estimate the mean extinction $\tau_{795} = -\ln(I/I_0)$ on each night.

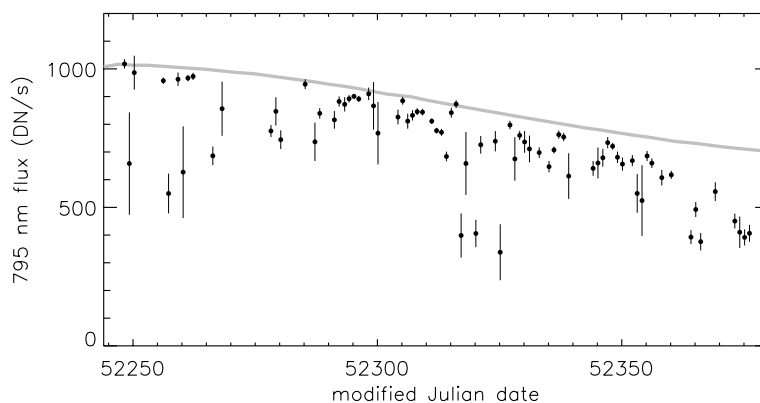


Figure 7.6: Titan’s raw 795 nm instrumental flux over 81 nights. A simple model of the predicted flux, multiplied by an arbitrary scaling factor, is shown as a gray line. Error bars indicate the 1- σ standard deviation of the raw flux on each night, not the uncertainty in the mean.

Figure 7.7 displays the observed nightly-mean flux ratios of Titan with respect to the 795 nm extinction τ_{795} . While the 750/795 nm ratio displays no correlation with extinction, the 825/890 nm and 795/890 nm clearly do. This may be due to atmospheric H₂O absorptions within the passbands of the 890 nm and possibly the 825 nm filters, which increase in opacity on cloudy nights. No known H₂O bands are included in the 750 and 795 nm filter passbands. Regardless of its precise cause, we correct for this systematic reddening of Titan by performing a linear fit to the observed values of these two flux ratios, and correcting

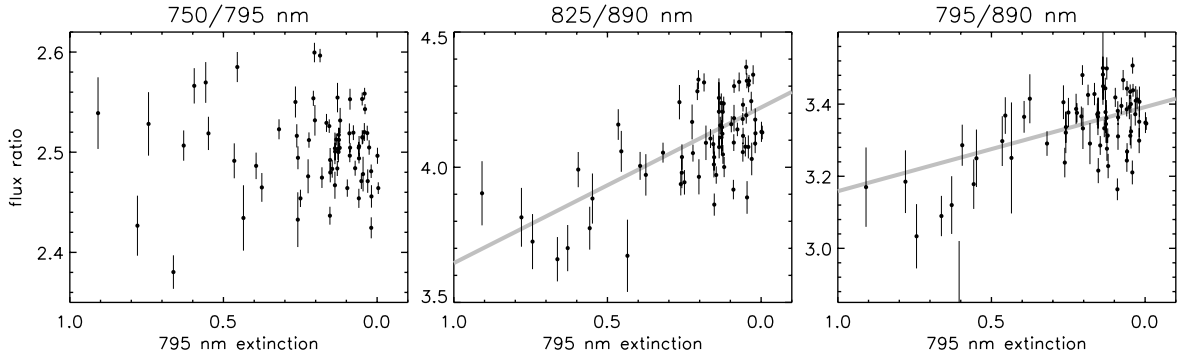


Figure 7.7: Ratios of Titan’s flux in various filters, displayed with respect to the mean 795 nm extinction on that night. the 825/890 nm and 795/890 nm flux ratios show a clear dependence on extinction, probably due to variability of H₂O bands in the 890 and possibly the 825 nm filters. No similar effect is seen in the 750/795 nm flux ratio.

their value in the subsequent discussion as follows.

$$f'_{825/890} = f_{825/890} + 0.576\tau_{795} \quad (7.1)$$

$$f'_{795/890} = f_{795/890} + 0.233\tau_{795} \quad (7.2)$$

We present a time series of the corrected flux ratios over the entire 4 month duration of the project in Fig. 7.8, and display them with respect to Titan’s orbital phase in Fig. 7.9. The 750/795 nm and 825/890 nm show a clear dependence on orbital phase, with Titan’s leading hemisphere relatively brighter than the trailing hemisphere. This is consistent with all previous observations of Titan’s surface, and demonstrates the sensitivity of these filters to light scattered from Titan’s surface. Though we clearly detect Titan’s hemispheric surface albedo contrast in the 750/795 nm flux ratio, its amplitude is low (2% peak-to-peak) due to the high optical depth of the overlying haze. The observed lightcurve amplitude increases to 5% in the 825 nm spectral window, which seem consistent with the 8% amplitude measured by ? through the 1.1 μ m window. As expected, the 795/890 nm flux ratio exhibits no statistically significant dependence on orbital phase.

7.4 Analysis

There is clearly more scatter superimposed on the repeating lightcurve than expected from the uncertainties which we estimate for the individual nightly-mean flux ratio measurements.

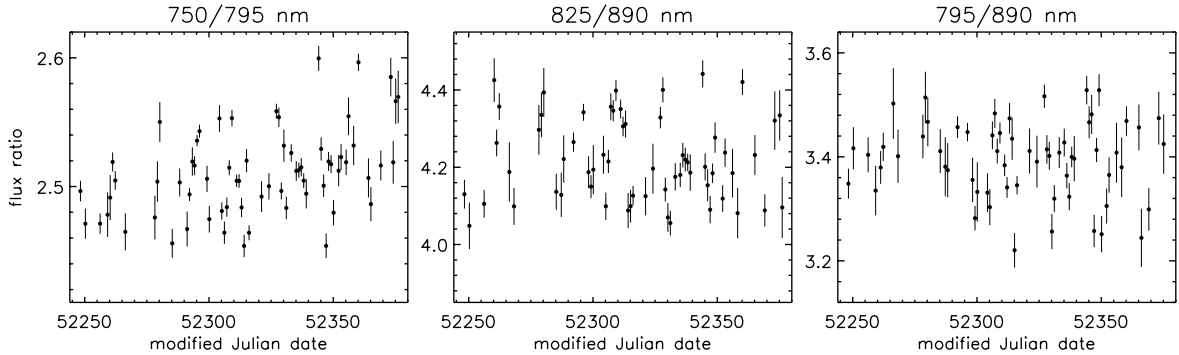


Figure 7.8: Titan’s nightly-mean flux ratio, with respect to date, in three filter combinations. 750/795 nm and 825/890 nm provide two independent estimates of the albedo of the lower atmosphere and surface, with respect to the overlying haze. Surface albedo, tropospheric clouds, and gradual changes in the color of the overlying haze might all contribute to these two ratios. The 795/890 nm CH_4 band ratio is insensitive to albedo variations below Titan’s tropopause. The same measurements are displayed with respect to Titan’s orbital phase in Fig. 7.9

This scatter could be due to a varying bias in the measured flux ratios (such as a variable spectral slope imposed by the Earth’s atmosphere) or to temporal variability of the albedo of Titan’s surface, lower atmosphere (clouds), or stratospheric haze. To distinguish between these possible contributors, we subtract from the observations an *ad hoc* lightcurve model, determined by fitting a 4th-order Fourier series to the phased 750/795 nm and 825/890 nm flux ratios. The corrected surface-sensitive flux ratios are displayed in Fig. 7.10. A clear trend can be seen in the 750/795 nm flux ratio, which increases by 3% over the 4 months of observation. No comparable long-term trend is seen in either the corrected 825/890 nm flux ratio or the 795/890 nm CH_4 band ratio.

If a gradual decrease in Titan’s 795 nm albedo were responsible for the trend in the 750/795 nm flux ratio, then we would expect the 795/890 nm CH_4 band ratio to increase by approximately the same magnitude. Such a result would not occur if Titan’s albedo at 890 nm were decreasing at the same rate, but in that case we would note a comparable increase in the 825/890 nm albedo, which is clearly not seen. We must therefore conclude that Titan gradually brightened at 750 nm, with respect to the longer wavelength filters. This trend is consistent with the photometric results of Lockwood *et al.* at shorter wavelengths, reported in Lorenz *et al.* (1999), who observed Titan’s “blue” albedo to rise at twice the rate of the “yellow” during 1972–1975, one Titan year previous. These seasonal

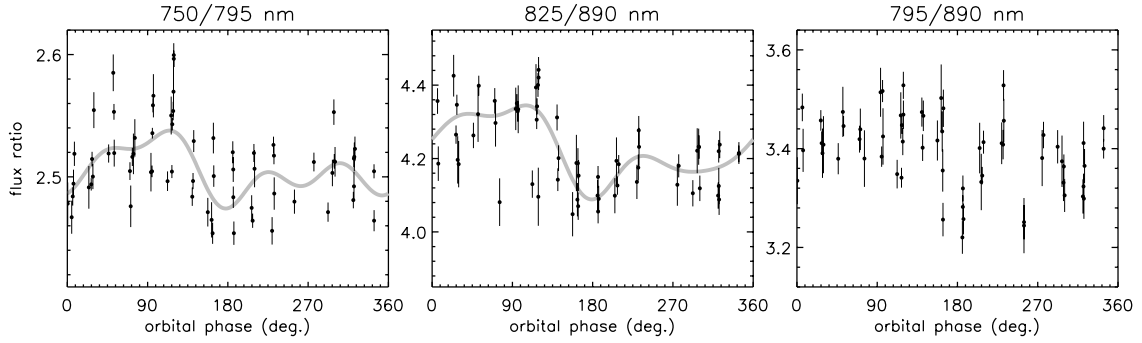


Figure 7.9: Titan’s nightly-mean flux ratio, with respect to orbital phase, in three filter combinations. Titan’s repeating lightcurve is approximated by the gray line, a least-squares fit 2nd-order Fourier series. The 795/890 nm CH₄ band flux ratio displays no statistically significant repeating lightcurve.

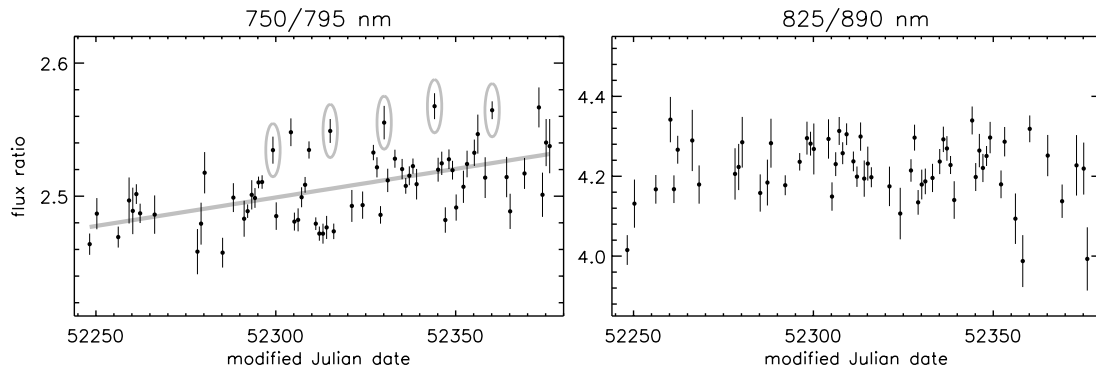


Figure 7.10: Titan’s nightly-mean flux ratio, corrected for the repeating surface albedo Fourier series with Titan’s orbital period has been subtracted. A clear trend can be seen in the 750/795 nm ratio, indicated by the linear fit in gray. Occasional brightenings of Titan’s surface or lower atmosphere which appear to repeat at precisely the orbital period are marked with gray ovals.

albedo variations have been interpreted as being caused by the modification of the size distribution of the haze on the most visible (summer) hemisphere of Titan by meridional transport (Lorenz *et al.*, 1999). In short, though we do detect photons from Titan’s surface at 750 nm, they are highly diluted by sunlight scattering off the optically thick haze, which was gradually brightening throughout the period of observation.

Besides this linear increase in the 750/795 nm flux ratio, we cannot conclusively identify any transient change in the flux ratios sensitive to the albedo of Titan’s surface or lower atmosphere. Several suggestive features in the data do merit closer attention, however. We twice observed brightenings of the 750/795 nm flux ratio, by $> 3\sigma$ over the expected

mean lightcurve value, which repeated at Titan’s orbital period. These observations in question are highlighted in Fig. 7.10. Unexpectedly high surface/lower atmosphere albedos were detected on 25 January, 10 and 25 February, and 11 and 27 March 2002, on which Titan’s orbital phase was 186.0, 185.5, 163.7, 119.4, and 119.4, respectively. We have not highlighted every $3\text{-}\sigma$ deviation from the gradual brightening trend, but it may be significant that in these 5 cases, possible abnormal brightenings appear to repeat at the orbital period.

There are similarly suggestive indications of variability in the lower atmosphere and surface in the corrected 825/890 nm flux ratio, as the values gradually increase to a maximum near MJD 52305 (31 January 2002), then decrease somewhat before increasing to a second maximum near MJD 52335 (2 March 2002), before becoming too noisy to follow such subtle trends. However, these suggestive features in the 750/795 nm and 825/890 nm ratios do not appear to correlate, and we therefore cannot confidently claim to have detected any changes in the albedo of Titan’s lower atmosphere and surface besides the unchanging surface lightcurve, on the basis of the C-14 photometry alone.

There are further reasons believe that the apparent lightcurve variability may not be due to changing clouds in Titan’s troposphere. Recent nightly imaging of Titan with the Palomar adaptive optics (AO) system has revealed that the clouds currently account for only 0.4–1.3% of Titan’s $2.0\ \mu\text{m}$ flux, corresponding to 3–8% of the present peak-to-peak lightcurve amplitude (Ch. 6). If the contrast of surface features which cause Titan’s lightcurve is similar at 750–825 nm and $2.0\ \mu\text{m}$, then we expect the clouds to have a similar photometric effect relative to the measured lightcurve amplitude in the visible. This is well below the $1\ \sigma$ uncertainties of the measured 750/795 and 825/890 nm flux ratios. Only if the nightly clouds observed with the Palomar AO system were optically thin and composed of small ($< 2\ \mu\text{m}$) droplets, or if the surface feature contrast were far lower in the visible, would the AO-imaged clouds be detectable in the C-14 photometry.

7.5 Conclusions

We attempted to detect the photometric signature of transient clouds in Titan’s troposphere, using nightly narrow-band photometry on a 14-inch telescope on the Caltech campus. Though we clearly detect the repeating lightcurve of Titan’s surface at 750 and 825 nm, transient brightenings due to clouds could not be conclusively identified. The technique

used remains promising, however, and implementation on a larger telescope or at a drier site might provide the signal-to-noise improvement necessary to achieve this project's goals.